Korean Journal of Remote Sensing, Vol.24, No.3, 2008, pp.223~233

Rigorous Modeling of the First Generation of the Reconnaissance Satellite Imagery

Sung-Woong Shin*† and Tony Schenk**

*Spatial Information Research Team, ETRI, KOREA, **Dept. of CEEGS, The Ohio State University, U.S.A.

Abstract : In the mid 90's, the U.S. government released images acquired by the first generation of photo reconnaissance satellite missions between 1960 and 1972. The Declassified Intelligent Satellite Photographs (DISP) from the Corona mission are of high quality with an astounding ground resolution of about 2 m. The KH-4A panoramic camera system employed a scan angle of 70° that produces film strips with a dimension of 55 mm × 757 mm. Since GPS/INS did not exist at the time of data acquisition, the exterior orientation must be established in the traditional way by using control information and the interior orientation of the camera. Detailed information about the camera is not available, however. For reconstructing points in object space from DISP imagery to an accuracy that is comparable to high resolution (a few meters), a precise camera model is essential.

This paper is concerned with the derivation of a rigorous mathematical model for the KH-4A/B panoramic camera. The proposed model is compared with generic sensor models, such as affine transformation and rational functions. The paper concludes with experimental results concerning the precision of reconstructed points in object space. The rigorous mathematical panoramic camera model for the KH-4A camera system is based on extended collinearity equations assuming that the satellite trajectory during one scan is smooth and the attitude remains unchanged. As a result, the collinearity equations express the perspective center as a function of the scan time. With the known satellite velocity this will translate into a shift along-track. Therefore, the exterior orientation contains seven parameters to be estimated.

The reconstruction of object points can now be performed with the exterior orientation parameters, either by intersecting bundle rays with a known surface or by using the stereoscopic KH-4A arrangement with fore and aft cameras mounted an angle of 30°.

Key Words : Satellite Imagery, DISP Images, Corona, Panoramic Camera.

1. Introduction

During the past few years, several high-resolution space-borne imaging systems have been launched and others will likely follow. The goal of mapping from space has become a reality.

High-resolution mapping from space is not exclusively related to recent technology, however. In fact, it goes back to the early 1960s when Corona, the first satellite imaging system, was developed and

Received June 1, 2008; Revised June 15, 2008; Accepted June 19, 2008.

† Corresponding Author: Sung-Woong Shin (sshin@etri.re.kr)

successfully used in a highly classified program. The Corona camera delivered photographs with a resolution of 2 m (a feat that only very recently has been surpassed). The veil on the super secret reconnaissance program was lifted in 1995 by an executive order. The declassified Corona imagery sets the clock of high-resolution mapping back to 1960. Almost one million images are now available to the public.

The Corona panoramic films (format 5.54 cm × 75.69 cm) have a remarkable resolution of about 2m. The polyester film base offers high stability. Thus, one can reasonably expect positional accuracies of features comparable to the resolution. This paper addresses the issue of determining positions in object space from measured points on Corona imagery as accurately as possible. The next section provides background information about the Corona program, including specifications about the camera and film. In Sec. 3, we describe the mathematical model for recovering the exterior orientation of the panoramic camera from control features in object space. This is necessary because the Corona missions were flown before the advent of GPS/INS. We also describe how to determine accurate positions of points in object space. We have performed several experiments with synthetic and real data to examine the feasibility of our proposed approach. Sec. 4 reports about some of the experiments. We conclude the paper with a brief summary about the major findings and point to future research related to the Corona imagery.

2. Background

Two presidential orders had a great impact on reconnaissance from space. The approval of the Corona project by President Eisenhower in 1958 marked the beginning of the first satellite imaging reconnaissance system ever built. However, due to its highly secretive character, it benefited only a rather small group in the intelligence community. The second presidential order related to Corona was issued 37 years later by President Clinton, which resulted in the declassification of the Corona imagery, including related documentation. This order benefited all those interested in using the high resolution imagery.

This section provides background information about the Corona project, the cameras used, and the declassified images. For a more detailed account on Corona, the reader is referred to a previous report (McDonald, 1997).

1) Corona reconnaissance project

The Corona project started officially in February 1958 and continued until May 25, 1972, the day of the last mission launch. The project was jointly managed by the CIA and the US Air Force, involving a number of industrial partners, among them Lockheed as the prime contractor and responsible for the Agenda spacecraft, and Fairchild and Itek that were responsible for the Corona cameras.

The principle idea of Corona was to photograph targets of interest with a high resolution camera, and eject the exposed film in a capsule so that it can be retrieved after the mission. To achieve this goal, a reentry vehicle was designed that contained the thermally protected film capsule. The reentry vehicle was equipped with a retro-rocket, attitude control system, telemetry link, and parachutes. Mid-air recovery of the capsule was accomplished by C-130 airplanes that flew above the capsule, caught it with a line and hooks, and hauled it into the open cargo area. If mid-air recovery failed, a back-up water recovery with helicopter and ship would secure the capsule.

The capsule recovery system became a major challenge. It was not before the ninth mission that the first capsule with a film was successfully recovered (August 1960). From this moment, the reliability of

Corona greatly improved. Out of 121 missions, 95 were successful. From 1963 to 1972, 69 missions were launched and only four ended unsuccessfully.

2) Corona cameras

Corona's reconnaissance cameras are referred to by the designator "KH" (from KeyHole). Fairchild manufactured the first two cameras, KH-1 and KH-2, that were flown on five successful missions from 1960 to 1961. Other Corona cameras included KH-3 (operated from 1961-1962), KH- 4 (1962-1963), KH-4A (1963-1969), and KH-4B (1967- 1972), all designed, revised and manufactured by Itek. On the majority of the 95 successful Corona missions, the KH- 4, KH-4A and KH-4B cameras have been used. These three cameras are very similar and we summarize their most important properties.

The KH-4 is a twin panoramic cameras with a convergence angle of 30°. The lens system employs a Petzval configuration with five positive lenses and a focal length of 609.6 mm. The lens barrel is about 914.4 mm and the distance from the first lens to the film is 1219.2 mm, resulting in a relatively bulky system. The lens constantly rotates about its rear nodal point and so does the slit that scans the image to the film. The film format is 5.54 cm × 75.69 cm and the scan angle is about 70°. The film base is polyester and the film load capacity of KH-4A and KH-4B is 9753 m, allowing a mission life of up to 19 days. In longer missions, the film would be ejected twice. The f/3.5 aperture accommodates relatively slow film. Laboratory resolution tests rendered 280 lp/mm under high contrast conditions and 175 lp/mm for medium conditions. Under operational conditions, up to 160 lp/mm were reached. This translates to a ground resolution of 2.8 m for orbits as low as 148 km. In order to achieve this resolution, image motion compensation (IMC) is essential. During the scan time, the platform moves and the Earth rotates. The Corona cameras compensated these anticipated movements by rotating the optics synchronous to the scan. The magnitude of the IMC was programmed and entered into the control unit prior to a mission.

Panoramic cameras are ideal for reconnaissance purposes. For one, the ground coverage is impressive. For example, the KH-4 camera scan angle of 70° produces a swath width of approximately 231 km. Moreover, the resolution is uniform with respect to radiometric and geometric distortions. These advantages come at the cost of a more complex imaging geometry. It stands to reason to expect a positional accuracy of measured features comparable to the resolution. That is, the position of well identified points should be 2 m in object space. With this goal in mind, Sec.3 proposes a suitable mathematical model.

3) Declassified imagery

The second presidential order related to Corona had and still continues to have a great impact on the mapping community. The US Geological Survey (USGS) is charged with archiving and distributing the declassified imagery. The EROS Data Center in Sioux Falls stores and disseminates over 866,000 images.

Access to the DISP catalog is facilitated by browse images (JPEG) that can be viewed on-line before ordering the films. Information about the images, such as geographic area and date, is also accessible through Internet.

The declassified intelligence satellite photographs (DISP) provide exciting opportunities. Earth science applications in particular benefit from the high quality images. Research related to change detection, for example urban expansion, ice sheet dynamics, soil erosion use DISP images to establish a baseline in time series studies (Csatho *et al.*, 1999; Thomas *et al.*, 2000; Csatho *et al.*, 2002).

Several studies have demonstrated the feasibility of using Corona KH-4A and KH-4B panoramic imagery for earth science research (Sohn, 1998; Kim, 1999; Altmaier and Kany, 2002; Sohn 2004). However, previous studies applied approximate sensor model [e.g., 2D polynomial transformation (Sohn, 1998; Kim, 1999)] to reconstruct the object points. Recently, a couple of studies were conducted to generate Digital Elevation Model (DEM) using a stereo pairs of Corona KH-4B images (Altmaier and Kany, 2002; Sohn 2004). These studies used ERDAS IMAGINE OrthoBASE Pro module, which is designed for frame camera imagery, to create DEM (Altmaier and Kany, 2002) and ortho-rectified images (Sohn, 2004). Hence, we suggest a rigorous model which describes the physical panoramic sensor characteristics and assures the robustness of the reconstructed object points.

3. Mathematical model for Corona KH-4A/B imagery

In order to determine object space positions of features measured on Corona images, the exterior orientation must be known. For the panoramic stereo cameras KH-4A and KH- 4B, the exterior orientation comprises the position of the perspective center and the attitude of the camera at any instance an image element is formed. We consider a slit as such an elementary image. Consequently, a Corona film strip has theoretically an infinite number of exterior orientation parameters.

During the Corona project, the exterior orientation was derived from orbit information and information obtained from auxiliary cameras, such as stellar and horizon cameras. Since necessary information for a precise exterior orientation is not always readily available, we propose a solution that is independent from orbital and star tracker data. The solution is based on known information in object space, such as control points and control features.

1) Indirect exterior orientation with control features

The collinearity model establishes a convenient relationship between image and object space by enforcing the condition that the perspective center, a point in object space and its image are on a straight line. This simple condition holds as long as the camera (perspective center and image) and the object point remain constant during the time of exposure. In the case of a panoramic camera, this is only true for a fixed slit position. We derive in the following the collinearity model for the slit at time t and then generalize for the entire strip. The term "strip" is here used to refer to one scan sweep of the panoramic camera.

Let O - XYZ be the object space coordinate frame, and let C_t - uvw be the camera coordinate frame with the origin at the perspective center C_t at scan time t. As illustrated in Fig. 1, the v-axis is parallel to the flight direction and the w-axis is pointing near

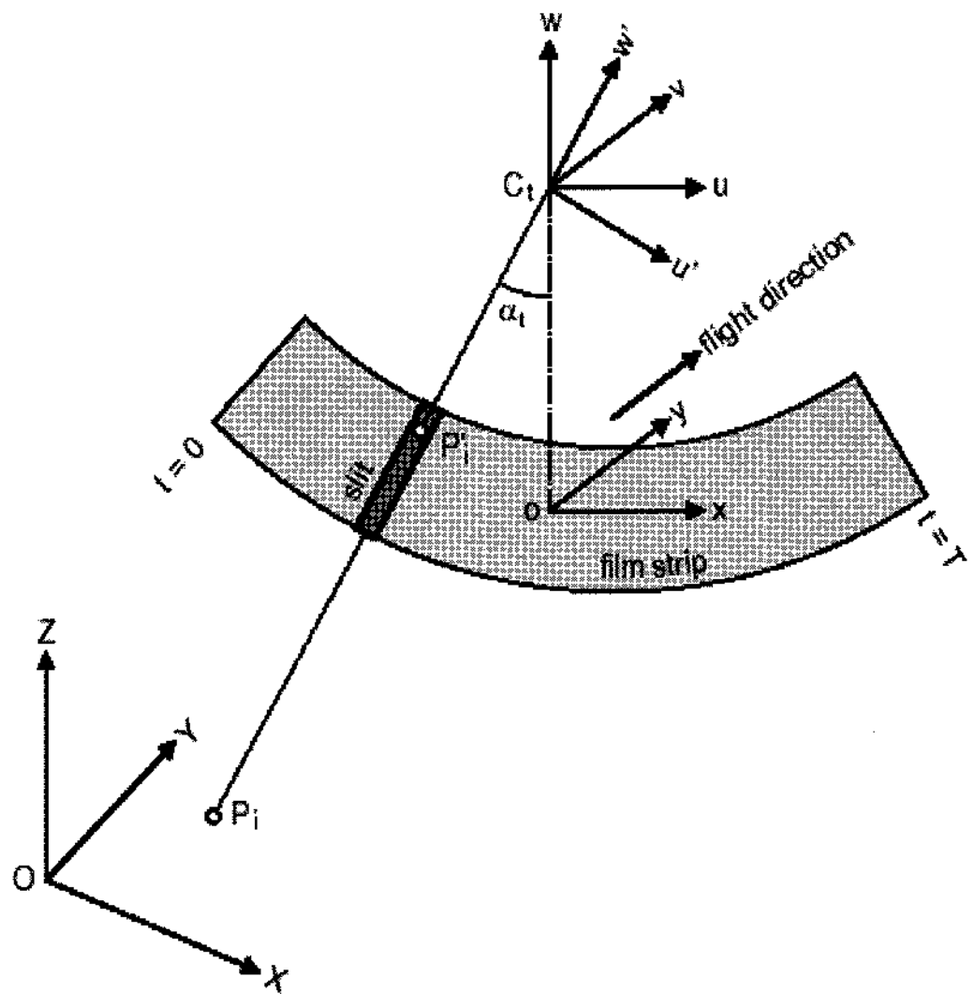

Fig. 1. Illustration of object space and image space coordinate frames.

vertical. Next, let C_t - $u'v'w'$ be the slit coordinate system with the negative w'-axis pointing to the position of the slit, again at scan time t. The origin and the v'-axis are identical to the respective quantities of the camera frame. Now, let o - xy denote the 2D image space coordinate frame with the origin, o, at the intersection of the w-axis with the positive film and with the x and y-axes parallel to the u and v-axes of the camera system, respectively. Then, the image coordinates (x_i, y_i) of a point P_i' are related to the camera coordinates by $[x_i\ y_i\ -f] = \lambda_i[u_i\ v_i\ w_i]$ with f the focal length and λ_i a scalar that differs from point to point. The slit moves from one end of the cylindrical image plane to the other one during the scan time T. This movement can also be described by angle α as indicated in Fig. 1. Thus, α_t [Radian] refers to the angle between the negative w-axis and slit position at scan time t. That is,

$$\alpha_t = x_i/f \qquad [1]$$

with x_i the image coordinate of point P_i'.

Let $\vec{P_i}$ the vector to object point P_i and $\vec{C_i}$ the vector to the perspective center at time t in the object space coordinate frame. The collinearity condition for points in slit t can now easily be expressed as

$$m_i' = R(t)(\vec{P_i} - \vec{C_i}) \qquad [2]$$

where, $m_i' = [0\ v_i'\ w_i'] = 1/\lambda_i[0\ y_i\ -f)$ which represents the image vector in the slit system. $R(t)$ is a 3D orthogonal rotation matrix that expresses the attitude (pitch, roll, azimuth) of the camera system with respect to the object space at scan time t. Let m_i be the image vector in the camera system. Then we have $m_i = R_\alpha m_i'$ where, R_α is a 3D orthogonal rotation matrix defined by a rotation of angle α_t about the v-axis as shown by the next equation

$$R_\alpha = \begin{pmatrix} \cos\alpha_t & 0 & \sin\alpha_t \\ 0 & 1 & 0 \\ -\sin\alpha_t & 0 & \cos\alpha_t \end{pmatrix} \qquad [3]$$

The collinearity condition for one swath can now be expressed as $m_i' = R_\alpha R(t)(\vec{P_i} - \vec{C_i})$, or

$$\begin{pmatrix} 0 \\ y_i \\ -f \end{pmatrix} = \frac{1}{\lambda_i} R_\alpha R(t) \begin{pmatrix} X_i - X(t) \\ Y_i - Y(t) \\ Z_i - Z(t) \end{pmatrix} \qquad [4]$$

Examining (4) reveals that the position, $[X(t)\ Y(t)\ Z(t)]$, and the attitude, $R(t)$, are functions of the scan parameter t. Theoretically, this leads to an infinite set of exterior orientation parameters for one film strip. To cope with this problem, we now introduce the following assumptions. During the short scan time we assume that the attitude of the stabilized satellite platform remains constant, that is, $R(t) = R$. For the same reason, the satellite trajectory is assumed to be smooth during the scan time. Let $d = [0\ D\ 0]$ be the vector that describes the change of the trajectory in the flight direction during one scan, where $D = v \cdot T$ is the travel distance, v the velocity of the satellite, and T is the total scan time of the panoramic camera. Then, any intermediate position is determined by multiplying d by a scalar, s that is proportional to t/T, or equivalently

$$s = x_i/L + 0.5 \qquad [5]$$

where, L represents the length of a film strip (see also Fig. 1). With all these assumptions, we can approximate the collinearity equations for one swath as follows:

$$\begin{pmatrix} 0 \\ y_i \\ -f \end{pmatrix} = \frac{1}{\lambda_i} R_\alpha \left(R \begin{pmatrix} X_i - X_O \\ Y_i - Y_O \\ Z_i - Z_O \end{pmatrix} - s \begin{pmatrix} 0 \\ D \\ 0 \end{pmatrix} \right) \qquad [6]$$

The scalar quantity λ_i can be eliminated by dividing the first two rows by the third row in equation [6]. This will leave us with two equations for every measured point P_i and a total of seven unknown parameters: $[X_O\ Y_O\ Z_O]$ which are the coordinates of the perspective center at the beginning of one swath; pitch, roll, and azimuth which are the three independent angles of the rotation matrix R; and, D which is the total travel distance of the satellite during one scan sweep. All other quantities in

equation [6] are known: $[X_i\ Y_i\ Z_i]$ which are the control point coordinates in object space; R_α which is defined by equation [1] and equation [3]; $[X_i\ Y_i]$ which are the measured image coordinates of the control points, and f which is the focal length.

Equation [6] serves as a starting point for determining the seven orientation parameters by an adjustment procedure, e.g. the least-squares adjustment method. Approximations which are necessary for the adjustment are readily obtained from the trajectory information that comes along with DISP imagery.

2) Space intersection

The KH-4 twin panoramic cameras provide stereo capabilities. The fore and aft cameras have a convergence angle of 30°. With the exterior orientation known using the mathematical model introduced above, we can now compute 3D positions of points in object space provided they are measured on overlapping fore and aft images. To obtain points, P_i, in object space we rearrange equation [6] as follows:

$$\begin{bmatrix} X_i \\ Y_i \\ Z_i \end{bmatrix} = \lambda_i R R_\alpha \begin{bmatrix} 0 \\ y_i \\ -f \end{bmatrix} + R^T \begin{bmatrix} 0 \\ s \cdot D \\ 0 \end{bmatrix} + \begin{bmatrix} X_O \\ Y_O \\ Z_O \end{bmatrix} \qquad [7]$$

The unknowns comprise the position $P_i = [X_i\ Y_i\ Z_i]$ and scalar λ_i. All other quantities are either measured or derived using exterior orientation parameters. Note that the x_i-coordinate does not appear explicitly. Measuring the same point P_i on the fore and aft images provides six equations with two scale parameters and three positions to be determined. Again, a least-squares adjustment solves this problem.

4. Experimental results

1) Data description

Experiments were carried out to test the proposed rigorous mathematical model for determining the exterior orientation of Corona images and ground coordinates through space intersection with real data sets. This section presents some of the results obtained with a fore and aft Corona KH-4A image stereo pair. Table 1 contains relevant mission data and other information. Film positives and metadata of an area in mid-Ohio were obtained from USGS.

Table. 1. Test data of Corona KH-4A images used for experiments

	Fore image	Aft image
Identifier	DS1026-1014DF005	DS1026-1014DA011
Time	October 29, 1965	
Ground coverage	17 km × 231 km (Approximately)	
# control pts	33	31
# check pts	33	33

The B/W films of a stereo pairs were scanned with a pixel size of 12 μm. Since the active scan areas of photogrammetric scanners are limited to aerial film formats (23 cm × 23 cm), the DISP film had to be scanned in portions. Using identical features in the overlapping area, a similarity transformation established a common film frame. Fig. 2 (c) depicts a small image patch, size 12 mm × 9 mm, demonstrating the high resolution of Corona images. The walkways in the oval feature of the image are approximately 3 m wide.

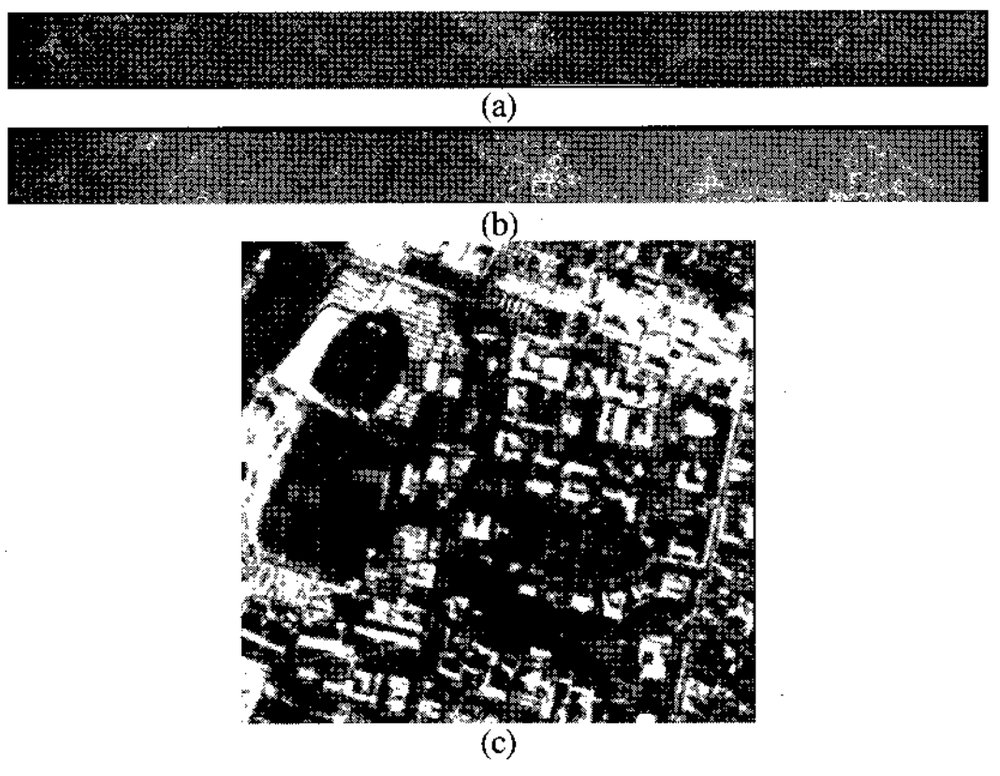

Fig. 2. Browse images of test images used for experiments; (a) Fore Image, (b) Aft image, and (c) an image patch of area indicated as a yellow rectangle in aft image.

2) Parameter estimation

The extended collinearity equations are the nonlinear functions so that it is necessary to input the initial approximate values of parameters for the adjustment process of the parameter estimation. The initial approximate values of parameters are obtained by the following steps:

(a) Approximations of X_o and Y_o are computed from the average of the ground coordinates of the four corner points described in the metadata of the CORONA KH-4A panoramic image published by the USGS EROS data center.

(b) Satellite altitude H could be used as the approximate value of Z_o.

(c) Conducting the 2-dimensional similarity transformation between the panoramic image coordinates and the ground coordinates of the selected points allows to obtain an initial approximation of azimuth.

(d) Approximation of pitch was obtained from the configuration of the CORONA KH-4A camera system (i.e., using the convergence angle between the fore camera and the aft camera).

(e) The approximate value of roll is assumed to be zero.

(f) The approximation of flight distance, which is the hardest part to get a good approximation, is assumed by trial and error until the solution converges.

The number of control points used in the estimation of the parameters is 33 points for fore image and 31 points for aft image. Fig. 3 shows the distribution of the control points and the check points in the object space. One can see that the scale of the easting-axis and the northing-axis is different. Since the test images are very long length and narrow width, the same scale of axes may bring the illegible to discern the configuration of the control points and

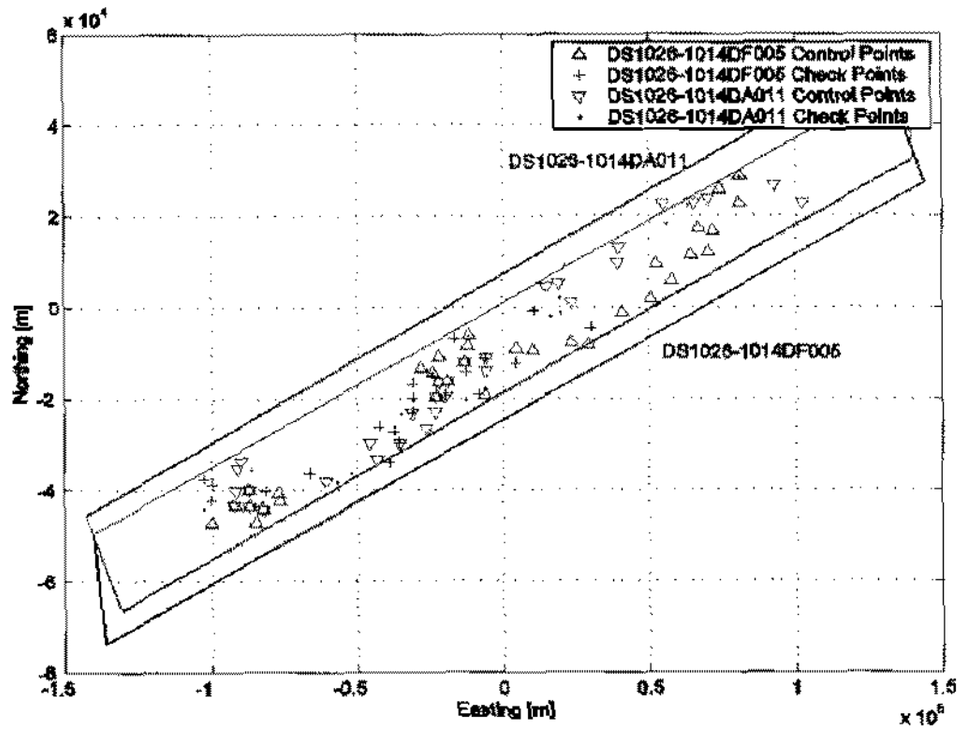

Fig. 3. The configuration of control points and check points used to parameter estimation.

Table 2. Estimated parameters of test images

Parameter	Fore image	Aft image
X_o (m)	-16432.20	14148.26
Y_o (m)	37321.89	-62495.86
Z_o (m)	197562.69	195474.03
Azimuth (deg.)	200.127	200.566
Pitch (deg.)	14.503	-16.375
Roll (deg.)	0.441	0.582
Moving Distance (m)	329.16	184.94

check points.

It should be noted that the twin cameras (fore camera and aft camera) did not acquire stereo pairs at the same acquisition time and the same exposure position due to the convergence angle of cameras. In addition, one can see the estimated moving distances of the fore and the aft images are different. The main reasons of these differences are due to the differences of the estimated sensor positions and the pitch angles.

The standard deviations of each parameters and the variance component of least squares adjustment are shown in Table 3.

After the parameters are estimated, it is possible to verify whether the estimated parameters are acceptable by exploring the RMSE (Root Mean Square Errors) of check points. Table 4 summarized the results of space intersection in terms of the RMSE

Table 3. Adjustment statistics of the estimated parameters of test images

Statistics	Fore image	Aft image
σ_{Xo} (lml)	0.750	0.476
σ_{Yo} (lml)	1.793	1.352
σ_{Zo} (lml)	0.493	0.411
$\sigma_{Azimuth}$ (lsec.l)	0.645	0.606
σ_{Pitch} (lsec.l)	1.856	1.404
σ_{Roll} (lsec.l)	0.261	0.262
σ_{D} (lml)	0.755	0.708
Variance Component	0.014	0.014

Table 4. RMSE of check points (compared with DRG*)

$RMSE_X$ (m)	$RMSE_Y$ (m)	$RMSE_Z$ (m)
6.15	5.62	12.34

* DRG(Digital Raster Graphs)

of check points.

In judging the results one should bear in mind that the check points have also errors, probably on the order of a few meters according to National Map Accuracy Standards 7.44 m for location and 1/3 of contour interval for elevation (Light, 1993). The elevation accuracy is slightly larger than expected. The convergence angle between fore and aft camera of 30° corresponds very nearly to a B/H (base height ratio) of a normal stereo model, which has a reasonable error propagation for elevations. However, the pitch error is considerably larger than the other angular errors. The pitch error directly affects elevations.

The intersection of points in object space depends on the exterior orientation. Thus, the results reported here also confirm the accuracies achieved with exterior orientation. In fact, the processes of indirect exterior orientation and object space reconstruction are closely intertwined and have the nice property that modeling errors, for example in the camera model, cancel out (Schenk, 1999).

3) Generation of Digital Elevation Model (DEM)

DEM is the one of the useful by-products in photogrammetric applications because it is used in a wide range of applications in the geosciences and geographic information systems. In this paper, DEM is generated by using a stereo pair of panoramic images and the space intersection algorithm. Fig. 4 briefly summarizes the steps of generating DEM

A total of 1800 tie points are identified on the sub part (Chosen as Area of Interest) of a stereo pairs by using the tie point collection module of ERDAS Imagine, and their ground coordinates are determined by using space intersection algorithm. The ground coordinates of these irregularly distributed points are sued as input for generating a regular grid of DEM. Fig. 5 shows the contour lines and shaded reliefs of the resultant DEM. The DEM spacing is 150 m for the easting and the northing.

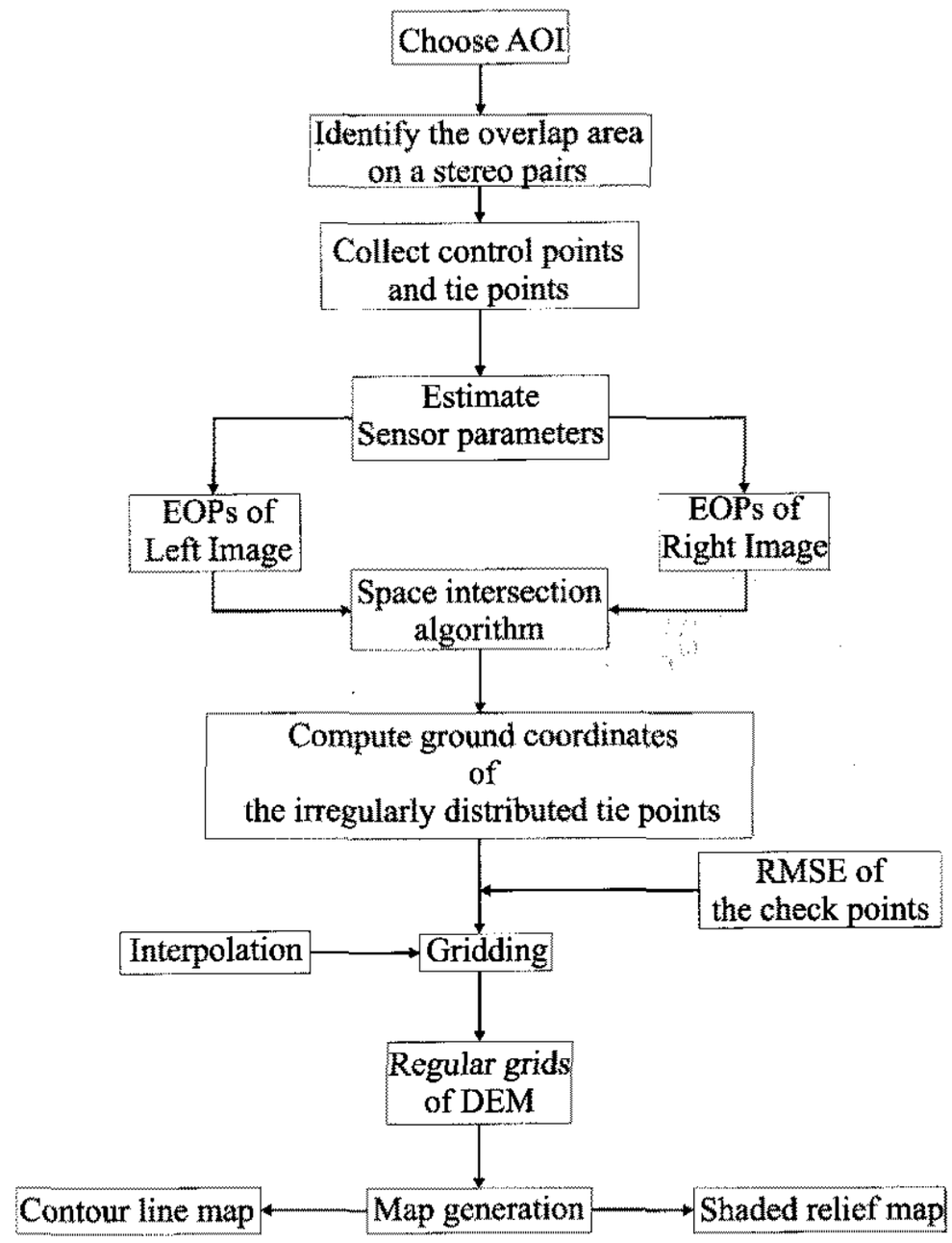

Fig. 4. Steps of DEM generation.

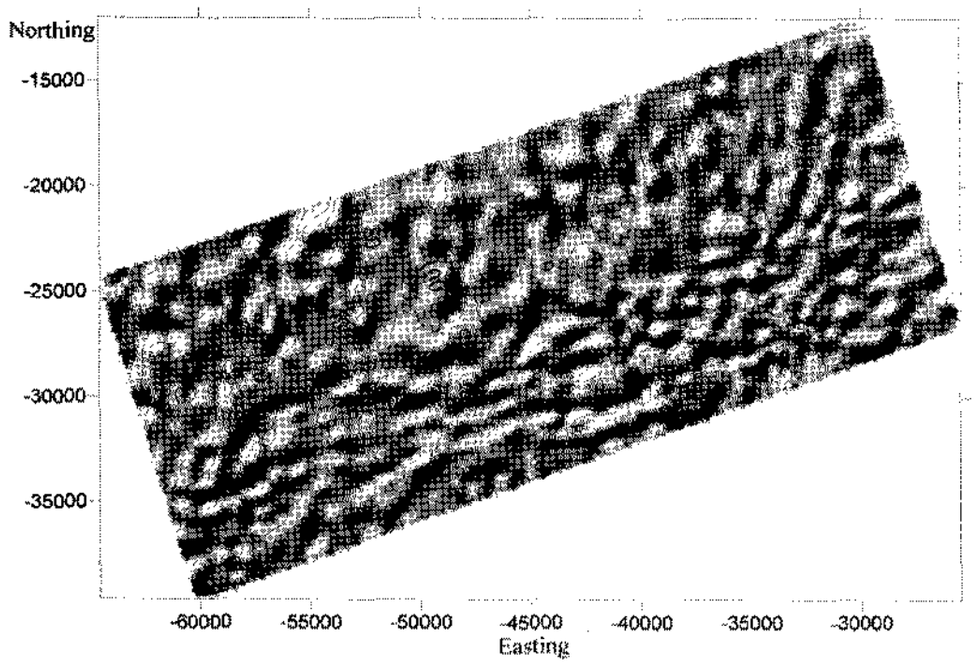

Fig. 5. Generated DEM.

4) Validation of suggested model by other generic models

We now compare the proposed approach with other image registration and reconstruction methods. Arguably, the most popular method to register images (image to image, image to map), is rubber sheeting. Here, a low order 2D polynomial is fitted through data points and control points in order to transform an image to another image or to a map. The polynomial coefficients are then used to transform non-control points. The simplest transformation in this scheme is an affine transformation. This approach cannot take topographic surfaces into account, nor can it cope with more complex camera models.

Recently, the Rational Function Model, RFM, has gained popularity. Its chief advantage is that higher order polynomials offer a way to circumvent an explicit modeling of the imaging sensors. This is of particular interest in situations where the camera model is unavailable. Several feasibility studies (Tao *et al.*, 2000; Dowman and Dollof, 2000) demonstrate the effectiveness of RFM.

For comparing the proposed rigorous mathematical model with the affine transformation model and the RFM, the fore and aft panoramic stereo pair images was registered to the same control points which was used for the exterior orientation. Next, the check point coordinates were transformed with the registration parameters to the object space and their locations were compared with the corresponding points measured on the digital map. Since the 3D reconstruction from a 2D image has one degree of freedom, we used the elevations from the map.

Table 5. Planimetric accuracy comparison of suggested model with other models

Image	2D Polynomial		RFM (2nd order)		Suggested Model	
	σ_x	σ_y	σ_x	σ_y	σ_x	σ_y
Fore	703.92	165.00	16.53	8.68	9.09	8.31
Aft	1038.20	109.21	35.55	8.12	8.78	9.48

Table 5 contains the result of this comparison test, expressed as standard deviations obtained from the differences between computed and known location. The affine model produced results with errors on the order of hundreds of meters. Unless applied to very small parts of the image where distortions resulting from the panoramic camera model and the topography are small, this simple form of rubber sheeting should not be used.

The 2nd order RFM model fares much better but is still inferior to our proposed approach. Not only are the errors larger, the outcome is less predictable and an optimal solution is often found experimentally. The results of suggested approach in Table 5 are consistent with those obtained from the stereo intersection.

5. Conclusions

The first generation of reconnaissance satellite images have a high resolution as well as wide area of coverage, which are a good source for the remote sensing and GIS applications. However, the complexity of panoramic camera sensor modeling leads people to use generic sensor models rather than a rigorous model for the registration of the Corona panoramic images into object space. This causes the

coarse approximate results derived from the Corona panoramic imagery without the benefits of the high resolution.

The goal of this study was to develop suitable algorithms that would allow the determination of positions of features in object space with an accuracy of few meters. In the case of Corona images the resolution is about 2~3 m. We have developed a two-step approach. First, the exterior orientation of the Corona camera is determined using known ground features, such as control points and control lines. The second step is concerned with intersecting features in object space from their measurements on stereo pairs. For this, the exterior orientation is a prerequisite.

We have demonstrated the feasibility of the proposed method with an example of a Corona stereo pair, covering an area of 13 km × 230 km in mid-Ohio. The film was digitized with a pixel size of 12 μm and the measuring accuracy is estimated to be one pixel. Multiplying the measuring accuracy with the scale (approx. 1:300,000) gives a crude but useful estimation of the accuracy of computed features in object space. The results obtained with 20 check points confirmed that this expected accuracy could be reached.

We also compared our approach with other methods, for example the affine transformation, and the rational function model. The affine transformation was found to be inadequate to cope with the geometry of panoramic cameras. The rational function model performs well but it required more control points.

We are currently performing more experiments with Corona panoramic imagery, including GPS check points, and matching stereo pairs for deriving DEMs automatically. Further studies are also being carried out to fuse Corona imagery with other sensory data for the purpose of change detection, especially long term change detection for the earth science fields.

Acknowledgements

This research was supported by a grant (07KLSG03) from Cutting-edge Urban Development - Korean Land Spatialization Research Project funded by Ministry of Land, Transport and Maritime Affairs.

References

Altmaier, A. and C. Kany, 2002. Digital surface model generation from CORONA satellite images, *ISPRS Journal of Photogrammetry and Remote Sensing*, 56: 221-235.

Csathó, B. M., J. F. Bolzan, C. van der Veen, T. Schenk, and D-C. Lee, 1999. Surface velocities of a Greenland outlet glacier from high-resolution visible satellite imagery, *Polar Geography*, 23: 71-82.

Csathó, B. M., T. Schenk, S. Shin, and C. J. van der Veen, 2002. Investigating long-term behavior of Greenland outlet glaciers using high resolution imagery, *Proceedings of IGARSS 2002* published on CD-ROM.

Dowman, I. and J. Dollof, 2000. An evaluation of rational functions for photogrammetric restitution, *ISPRS Intern. Archives*, 33(B3): 254-266.

Kim, K. T., 1999. *Application of Time Series Satellite Data to Earth Science Problem*, Master Thesis, Dep. of Civil and Environmental Engineering and Geodetic Science, The Ohio State University.

Light, D. L., 1993. The National Aerial Photography Program as a Geographic Information System Resource, *Photogrammetric Engineering and Remote Sensing*, 59(1): 61-65.

McDonald, R., 1997. *Corona between the Sun and*

the Earth, ASPRS, 5410 Grosvenor Lane, Bethesda, Md., p. 440.

Schenk, T., 1999. *Digital Photogrammetry*, 1st Edition, Vol. I, TerraScience, Laurelville, p. 383-386.

Sohn, H. G., 1998. Jakobshavn Glacier, West Greenland: 30 years of spaceborne observations, *Geophysical Research Letters,* 25(14): 2699-2702.

Sohn, H. G., G. H. Kim, and J. H. Yom, 2004. Mathematical modeling of historical reconnaissance CORONA KH-4B imagery, *The Photogrammetric Record*, 19(105): 51-66.

Tao, V., Y. Hu, B. Mercer, S. Schnick, and Y. Zhang, 2000. Image rectification using a generic sensor model-rational function model, *ISPRS Intern. Archives*, 33(B3): 874-881.

Thomas, R. H., W. Abdalati, T. Akins, B. Csathó, E. Frederick, P. Gogineni, W. Krabill, S. Manizade, and E. Rignot, 2000. Substantial thinning of a major east Greenland outlet glacier, *Geophysical Research Letters,* 27(9): 1291-1294.